A geostatistically based inverse model for electrical resistivity surveys and its applications to vadose zone hydrology

T.-C. Jim Yeh,[1] S. Liu,[1] R. J. Glass,[2] K. Baker,[3] J. R. Brainard,[2] D. Alumbaugh,[4] and D. LaBrecque,[5]

Received 24 January 2001; revised 16 May 2002; accepted 6 June 2002; published 6 December 2002.

[1] A sequential, geostatistical inverse approach was developed for electrical resistivity tomography (ERT). Unlike most ERT inverse approaches, this new approach allows inclusion of our prior knowledge of general geological structures of an area and point electrical resistivity measurements to constrain the estimate of the electrical resistivity field. This approach also permits sequential inclusion of different data sets, mimicking the ERT data collection scheme commonly employed in the field survey. Furthermore, using the conditional variance concept, the inverse model quantifies uncertainty of the estimate caused by spatial variability and measurement errors. Using this approach, numerical experiments were conducted to demonstrate the effects of bedding orientation on ERT surveys and to show both the usefulness and uncertainty associated with the inverse approach for delineating the electrical resistivity distribution using down-hole ERT arrays. A statistical analysis was subsequently undertaken to explore the effects of spatial variability of the electrical resistivity-moisture relation on the interpretation of the change in water content in the vadose zone, using the change in electrical resistivity. Core samples were collected from a field site to investigate the spatial variability of the electrical resistivity-moisture relation. Numerical experiments were subsequently conducted to illustrate how the spatially varying relations affect the level of uncertainty in the interpretation of change of moisture content based on the estimated change in electrical resistivity. Other possible complications are also discussed. *INDEX TERMS:* 0903 Exploration Geophysics: Computational methods, potential fields; 1869 Hydrology: Stochastic processes; 1875 Hydrology: Unsaturated zone; 1866 Hydrology: Soil moisture; 3260 Mathematical Geophysics: Inverse theory; *KEYWORDS:* geostatistical inverse model, electrical resistivity tomography, vadose zone, resistivity-moisture relation, spatial variability, sequential/successive linear estimator

Citation: Yeh, T.-C. J., S. Liu, R. J. Glass, K. Baker, J. R. Brainard, D. L. Alumbaugh, and D. LaBrecque, A geostatistically based inverse model for electrical resistivity surveys and its applications to vadose zone hydrology, *Water Resour. Res.*, *38*(12), 1278, doi:10.1029/2001WR001204, 2002.

1. Introduction

[2] The DC resistivity survey is an inexpensive and widely used technique for investigation of near-surface resistivity anomalies. It recently has become popular for the investigation of subsurface pollution problems [*National Research Council* (*NRC*), 2000]. In principle, it measures the voltage generated by a transmission of current between electrodes implanted at the ground surface. Apparent (bulk or effective) electrical resistivity is then calculated and used to interpret subsurface anomalies.

[3] Classical formulas for determining apparent electrical resistivity assume homogeneity, and the potential field is smooth because of its highly diffusive nature. Consequently, conventional interpretations of electrical resistivity survey data have been virtually ineffective for environmental applications, where electrical resistivity anomalies are subtle, complex, and multiscale. To overcome these difficulties, a contemporary electrical resistivity survey has been designed to collect extensive electric current and electric potential data sets in multi-dimensions. Without assuming subsurface homogeneity, a mathematical computer model is employed to invert the data sets to estimate the resistivity field, using a regularized optimization approach [e.g., *Daily et al.*, 1992; *Ellis and Oldenburg*, 1994; *Li and Oldenburg*, 1994; *Zhang et al.*, 1995]. However, the general uniqueness and resolution of the three-dimensional electrical resistivity inversion have not been investigated sufficiently thus far [*Carle et al.*, 1999; *NRC*, 2000].

[4] While the physical process is different, the governing equation for electric currents and potential fields created in the electrical resistivity survey is analogous to that for steady flow in saturated porous media. The mathematical solution to the inversion of an electrical resistivity survey is therefore similar to that of a groundwater hydrological survey. Groundwater hydrologists and reservoir engineers

[1]Department of Hydrology and Water Resources, University of Arizona, Tucson, Arizona, USA.
[2]Sandia National Laboratory, Los Alamos, New Mexico, USA.
[3]Idaho National Engineering and Environmental Laboratory, Idaho Falls, Idaho, USA.
[4]Department of Civil and Environmental Engineering, University of Wisconsin-Madison, Madison, Wisconsin, USA.
[5]MultiPhase Technologies, Sparks, Nevada, USA.

0043-1397/02/2001WR001204$09.00

have attempted to solve the inverse problem of flow through multidimensional, heterogeneous porous media for the last few decades [e.g., *Gavalas et al.*, 1976]. Extensive reviews on the inverse problem of subsurface hydrology and various solution techniques are given by *Yeh* [1986], *Sun* [1994], and *McLaughlin and Townley* [1996]. They concluded that prior information on geological structure, and some point measurements of parameters to be estimated are necessary to better constrain the solution of the inverse problem. A similar finding was also reported by *Oldenburg and Li* [1999] and *Li and Oldenburg* [2000] for the inverse problems in geophysics.

[5] Groundwater hydrologists also have used a multicomponent linear estimator (cokriging) to estimate the hydraulic conductivity field from scattered measurements of pressure head and hydraulic conductivity in saturated flow problems [*Kitanidis and Vomvoris*, 1983; *Hoeksema and Kitanidis*, 1984]. The popularity of cokriging is attributed to its ability to incorporate spatial statistics, point measurements of hydraulic conductivity, and hydraulic head into the estimation and to yield conditional mean estimates. Cokriging is also capable of quantifying the uncertainty associated with its estimate due to limited information and heterogeneity. *Kitanidis* [1997] articulated the differences between cokriging and the classical inverse methods in subsurface hydrology. Nevertheless, cokriging is a linear estimator and it is limited to mildly nonlinear systems, such as aquifers of mild heterogeneity, where the variance of the natural logarithm of hydraulic conductivity, $\sigma^2_{\ln K}$, is less than 0.1. When the degree of aquifer heterogeneity is large ($\sigma^2_{\ln K} > 1$), the linear assumption becomes inadequate. Therefore cokriging cannot take full advantage of the hydraulic head information to obtain a good estimate of hydraulic properties [*Yeh et al.*, 1996].

[6] To overcome this shortcoming, *Yeh et al.* [1995, 1996], *Gutjahr et al.* [1994], and *Zhang and Yeh* [1997] developed an iterative geostatistical technique, referred to as a successive linear estimator (SLE). In this technique, a linear estimator was used successively to incorporate the nonlinear relation between hydraulic properties and the hydraulic head. This method also employs a conditional covariance concept to quantify reductions in uncertainty due to the incorporation of subsequent information. *Yeh et al.* [1995, 1996] and *Zhang and Yeh* [1997] demonstrated that with the same amount of information, the SLE method revealed a more detailed hydraulic conductivity field than cokriging. *Hughson and Yeh* [1998, 2000] extended the SLE method to the inverse problem in three-dimensional, variably saturated, heterogeneous porous media. On the basis of the SLE algorithm, *Yeh and Liu* [2000] developed a sequential SLE technique for hydraulic tomography to process the large amount of data created by the tomography, and subsequently characterize aquifer heterogeneity. They investigated the effect of monitoring intervals, pumping intervals, and the number of pumping locations on the final estimate of hydraulic conductivity, and they established guidelines for a design of a hydraulic tomography test.

[7] In section 2 of this paper, we introduce the concept of stochastic representation of electrical resistivity tomography (ERT) inverse problems. In sections 3 and 4 we describe the development of a geostatistically based sequential SLE methodology for ERT inversion problems. Section 5 offers numerical examples that illustrate the usefulness of the new inversion approach, and describes the effects of geological structures on the layout of electrical resistivity surveys. The relation between the electrical resistivity and the moisture content of 25 soil cores were measured and analyzed for spatial variability in section 6. Impacts of spatial variability on the estimated changes in moisture content in the vadose zone, using ERT surveys were explored and discussed in section 7.

2. Stochastic Conceptualization of ERT Inverse Problems

[8] Assume that in a geological formation, the electric current flow induced by an electrical resistivity survey can be described by

$$\nabla \cdot (\xi(x)\nabla\phi(x)) + I(x) = 0, \tag{1}$$

where x is location, ϕ is electric potential [V], I represents the electric current source per volume [A/m^3], and ξ is the electrical conductivity [S/m], a reciprocal of the electrical resistivity, ρ [ohm m], which is assumed to be locally isotropic. The boundary conditions associated with (1) are

$$\phi|_{G_1} = \phi^* \qquad \xi(x)\nabla\phi \cdot \mathbf{n}|_{G_2} = q, \tag{2}$$

where ϕ^* is the electric potential specified at boundary G_1, q denotes the prescribed electric current per unit area, and $\mathbf{n}$ is the unit vector normal to the boundary G_2.

[9] The electrical conductivity or resistivity of geological media varies spatially due to inherent heterogeneous geological processes [*Sharma*, 1997]. One way to describe the spatial variability of the electrical conductivity is the stochastic representation approach, similar to that used in geohydrology for the variability of hydraulic properties of aquifers and vadose zones [see *Gelhar*, 1993; *Yeh*, 1998]. Specifically, the natural logarithm of the electrical conductivity, $\ln\xi(x)$, of a geological formation is to be considered as a stochastic process. The process is described in terms of an unconditional mean, $\langle \ln\xi(x) \rangle = \Sigma$ ($\langle\ \rangle$ denotes the expected value) and perturbations, $\chi(x)$, which have an infinite number of possible realizations, characterized by a joint probability distribution. Assuming that the perturbation is a second-order stationary stochastic process, its joint probability distribution can then be adequately represented by its unconditional covariance function, $\mathbf{R}_{\chi\chi}$. The covariance function essentially depicts the average spatial correlation structure (pattern) of the electrical conductivity of a field in the statistical sense. The use of the natural logarithm transformation is merely a mathematical convenience. Similarly, the electric potential field induced during an ERT survey can be considered as a stochastic process and presented by $\phi(x) = V(x) + v(x)$, where $V(x) = \langle \phi(x) \rangle$ and $v(x)$ are the unconditional perturbations of the electric potential.

[10] Suppose that there are electrical conductivity measurements (referred to as the primary variable or primary information) from borehole electrical resistivity surveys, $\chi_i^* = (\ln\xi(x_i) - \Sigma)$ where $I = 1, 2, \ldots n_\chi$, and n_χ is the total number of electrical conductivity measurements. From these measurements, we have estimated the mean and covariance function of the electrical conductivity field. An

ERT survey is then conducted, and we have collected m sets of n_v electric potential (perturbation) values, v_j*, where $j = n_\chi + 1, n_\chi + 2, \ldots, n_\chi + m \times n_v$. Hereinafter, they are referred to as secondary information. We then seek an inverse model that can produce the electric potential and electrical conductivity fields that preserve the observed electrical potential and electrical conductivity values at sample locations. In addition, the fields must possess the statistics (i.e., the mean and covariance function) describing their spatial variability, and also satisfy underlying physical processes (i.e., the governing electric potential equation). In a conditional probability concept, such an electric potential or electrical conductivity field is a conditional realization of $\phi(x)$ field or $\ln\xi(x)$ field, respectively, among many possible realizations of the ensemble. The conditional electrical conductivity fields of the ensemble can be expressed as the sum of conditional mean electrical conductivity and its conditional perturbation, i.e., $\ln\xi_c(x) = \Sigma_c(x) + \chi_c(x)$. The subscript c denotes the state of being conditioned. Similarly, the conditional potential fields can be written as $\phi_c(x) = V_c(x) + v_c(x)$. While many possible realizations of such conditional $\ln\xi(x)$ and $\phi(x)$ fields exist, the conditional mean fields (i.e., $\Sigma_c(x)$ and $V_c(x)$) are unique, although not necessarily exactly reflective of the true fields.

[11] One way to derive these conditional mean fields is to solve the inverse problem to obtain all possible conditional realizations of the electrical resistivity field. An average of the possible realizations will yield the conditional-mean electrical resistivity field (see *Hanna and Yeh* [1998] and others for geohydrology applications). An alternative to the above is to solve the inverse problem in terms of the conditional mean equation.

[12] By substituting the conditional stochastic variables into the governing electric potential equation (1) and taking the expected value, the conditional-mean equation takes the form

$$\nabla \cdot [\Sigma_c(x)\nabla V_c(x)] + \nabla \cdot \langle \chi_c(x)\nabla v_c(x)\rangle + I(x) = 0. \quad (3)$$

In equation (3), the current source, $I(x)$, is considered deterministic. Notice that the true conditional mean $\Sigma_c(x)$ and $V_c(x)$ fields do not satisfy the continuity equation (3) unless the second term involving the product of perturbations is zero. This term represents the uncertainty because of a lack of information of the two variables at locations where measurements are not available. The uncertainty will vanish under two conditions, namely, (1) all the electrical conductivity values in the domain are specified (i.e., $\chi_c(x) = 0$), or (2) all the electric potential values in the domain are known (i.e., $v_c(x) = 0$). In practice, these two conditions will never be met, and evaluation of this term is intractable at this moment. Consequently, in the subsequent analysis we will assume this term is proportional to the conditional mean electric potential gradient such that we can rewrite the mean equation as

$$\nabla \cdot [\Sigma_{ceff}(x)\nabla V_c(x)] + I(x) = 0. \quad (4)$$

This conditional mean equation has the same form as equation (1) but variables are expressed as the conditional effective electrical conductivity, $\Sigma_{ceff}(x)$, and conditional mean electric potential field, $V_c(x)$. The conditional effective electrical conductivity thus is a parameter field that combines the conditional mean electrical conductivity $\Sigma_c(x)$ and $\langle \chi_c(x)\nabla v_c(x)\rangle(\nabla V_c(x))^{-1}$. According to this concept, the conditional effective electrical conductivity is a parameter field that agrees with the electrical conductivity measurements at sample locations, and it yields a conditional mean electric potential field that preserves values of electric potential measurements when it is employed in the forward model (4), subject to boundary conditions (2). On the basis of this concept, an optimal inverse solution to equation (4) seeks the conditional effective electrical conductivity field. The successive linear estimator (SLE) approach is appropriate for this purpose.

3. Geostatistically Based SLE Inversion for ERT

[13] Below we present a brief description of the SLE algorithm. A detailed discussion of the algorithm is given by *Yeh and Liu* [2000]. The SLE algorithm, in general, consists of seven steps. Step 1 starts with a linear estimator using primary and secondary information to estimate the value of the primary variable at j locations where no information is available about the variable:

$$\hat{\boldsymbol{\chi}} = \boldsymbol{\lambda}_\chi^T \boldsymbol{\chi}^* + \boldsymbol{\lambda}_v^T \mathbf{v}^*, \quad (5)$$

where $\hat{\boldsymbol{\chi}}$ is a $\boldsymbol{j} \times \boldsymbol{1}$ vector of the estimated primary variable, χ, (i.e., the estimated χ_c) at j locations and χ*, and $\mathbf{v}$* are available information about the primary and secondary variables (i.e., electrical conductivity, and potential measurements, respectively) at n_d ($n_d = n_\chi + n_v$) sample locations. The $n_d \times j$ matrix, λ_χ, and $n_v \times j$ matrix, λ_v, are the cokriging weights applied to the primary and the secondary information. They are related to the spatial covariance function of the primary and the secondary variable (i.e., $\mathbf{R}_{\chi\chi}$ and $\mathbf{R}_{vv}$, respectively) as well as the cross-covariance between the primary and secondary variables, $\mathbf{R}_{\chi v}$. The covariance function, $\mathbf{R}_{\chi\chi}$, of the primary variable is prescribed a priori, and $\mathbf{R}_{vv}$, and $\mathbf{R}_{\chi v}$ are calculated using a first-order analysis and the given $\mathbf{R}_{\chi\chi}$ [see *Yeh and Liu*, 2000]. To include the uncertainty due to measurement errors associated with primary and secondary information, additional variances can be added to the diagonals of $\mathbf{R}_{\chi\chi}$ and $\mathbf{R}_{vv}$. The weights are then obtained from the solution of a cokriging system of equations. In step 2, the covariance of the primary variable is modified to reflect effects of the available information. That is,

$$\mathbf{R}_{\chi\chi}^{(r+1)} = \mathbf{R}_{\chi\chi}^{(r)} - \breve{\mathbf{R}}_{\chi\chi}^{(r)} \boldsymbol{\lambda}_\chi - \mathbf{R}_{v\chi}^{(r)} \boldsymbol{\lambda}_v \quad (6)$$

where $\breve{\mathbf{R}}_{\chi\chi}^{(r)}$ is a $j \times n_d$ subset of $\mathbf{R}_{\chi\chi}^{(r)}$, covariance of χ. The superscript in parentheses is the iteration index and $r = 0$ at this time. In step 3, the newly estimated variable field from equation (5) is used to simulate the electric potential field, v, using the forward model (4). In step 4, the conditional covariances, $\mathbf{R}_{vv}^{(r+1)}$ and their cross-covariance, $\mathbf{R}_{v\chi}^{(r+1)}$ are updated using a first-order analysis. For step 5, these newly evaluated covariances and cross-covariances compute new weights, λ_v, using

$$\mathbf{R}_{vv}^{(r)} \boldsymbol{\lambda}_v = \mathbf{R}_{v\chi}^T. \quad (7)$$

Step 6 is where the new weights, along with the difference between simulated $\mathbf{v}^{(r)}$ and observed $\mathbf{v}^*$, are used to improve the estimate of the primary variable. That is,

$$\hat{\chi}^{(r+1)} = \hat{\chi}^{(r)} + \lambda_v^{(r)^T}\left(\mathbf{v}^* - \mathbf{v}^{(r)}\right). \quad (8)$$

In equation (8), $\hat{\chi}^{(r)}$ represents the conditional primary variable estimate at iteration r. In step 7, the weights are then used to update conditional covariances for the next iteration using

$$\mathbf{R}_{\chi\chi}^{(r+1)} = \mathbf{R}_{\chi\chi}^{(r)} - \mathbf{R}_{v\chi}^{(r)}\lambda_v. \quad (9)$$

This newly updated primary variable field (8) and the new conditional covariance (9) are used again in steps (3) and (4), followed by steps (5) through (7). Steps (3) through (7) are repeated until no improvement in the estimate of the primary variable is found (i.e., when the variance of the estimated primary variable stabilizes). Notice that parallel computing procedures can be implemented in many steps of SLE.

4. Sequential Inversion of ERT Surveys

[14] The above discussion describes the SLE method for the secondary information collected during one excitation (i.e., one current source location) in an ERT survey. The method can simultaneously include all the secondary information collected during all the excitations in an ERT survey; however, the system of equations, (7), can become extremely large and ill conditioned. Therefore stable solutions to the equations can become difficult to obtain [*Hughson and Yeh*, 2000]. To avoid this problem, the secondary information collected from excitations at different locations is used sequentially. Specifically, our sequential method starts the inversion with the secondary information collected from the excitation at one selected location. Once the estimated field converges to the given criterion, the newly estimated conditional effective primary field and its conditional covariance are used as prior information for the inversion of the next excitation. That is, the conditional effective χ is used to evaluate both the conditional mean v, and sensitivity matrix associated with the excitation at the new location. Using the first-order analysis, the sensitivity matrix and conditional covariance, $\mathbf{R}_{\chi\chi}$, yield the v covariance and its cross-covariance with χ, which are subsequently employed to derive the new weights. With the conditional mean of v, the new weights, and the observed v^*, equation (8) then produces a new estimate of the conditional effective χ, representing the estimate based on the information from the excitation at the new location. The iterative process (similar to steps (3) through (7)) is then used to include the nonlinear relation between v and χ. Once the solution converges and iteration stops, the same procedure is applied to the information of the next excitation. This sequential process continues until the data sets created from all the excitations are all used in the inversion.

[15] Our sequential approach uses the estimated electrical conductivity field and covariance, conditioned on previous sets of potential measurements, as prior information for the next estimation based on a new set of current source data. The conditional moments are propagated sequentially until all the data sets are fully utilized. Such a sequential approach thus allows accumulation of the vast amount of secondary information obtained from an ERT survey, while maintaining the system of equations to be solved at a manageable size and with the least numerical difficulties. *Vargas-Guzman and Yeh* [1999] provided a theoretical proof to show that such a sequential approach is identical to the simultaneous approach for linear systems. This sequential algorithm for hydraulic tomography was also tested and verified in sandbox experiments [*Liu et al.*, 2002].

5. Numerical Examples

[16] To demonstrate the ability of our inverse method for ERT, a vertical profile of a hypothetical vadose zone (200 cm $\times$ 10 cm $\times$ 200 cm) was created and discretized into 20 $\times$ 1 $\times$ 20 elements of 1000 cm^3. A stochastic random field generator [*Gutjahr*, 1989] was used to assign an electrical conductivity value to each element. The electrical conductivity field was assumed to have a geometric mean of 0.01261 [S/m] and a covariance with an exponential correlation structure and a variance of 0.5 for the natural logarithm of the electrical conductivity field. The correlation structure was anisotropic with a horizontal correlation of 240 cm and a vertical correlation scale of 20 cm. This anisotropic structure yielded a heterogeneous and stratified electrical conductivity distribution shown in Figure 1a.

[17] Two cases were examined to illustrate effects of stratification on an ERT array layout. In cases I, an ERT surface array is deployed on the hypothetical stratified formation, representing an ERT array parallel to stratification. In cases II, the same surface array is deployed on the surface of a formation (Figure 1b) identical to the hypothetical vadose zone in cases I but rotated counterclockwise 90°, representing an ERT array perpendicular to stratification.

[18] During both ERT surveys, a pole-pole array was used. Nineteen potential electrodes (triangles in Figures 1c, 1d, 1e, and 1f) and one current electrode (circle) were used during each survey. In this example, the current electrode was moved 4 times from one position to another to create four voltage/current data sets, in which each set consists of 19 potential measurements and one current measurement. Note that the graphic depicts four circles: Only one current electrode was used in each survey, but it was positioned at four different locations for the four surveys. The ERT surveys were simulated numerically using equation (1), assuming the surface to be a boundary with no electric current flux and the remaining three sides of the vadose zone to be prescribed electric potential boundaries.

[19] Once the voltage/current data sets became available and one electrical conductivity measurement was taken (square in Figures 1c and 1d), the sequential inverse approach was employed to estimate the electrical conductivity field. Figures 1c and 1d depict the estimated conditional effective χ fields for cases I and II, respectively. A comparison between Figures 1c and 1d shows that the same surface array results in better estimates at depths in case II than in case I. Similarly, Figures 1e and 1f show that the conditional variance (uncertainty of estimate) is smaller at depths in case II than in case I. The conditional variance at a location indicates the uncertainty of the estimate at the

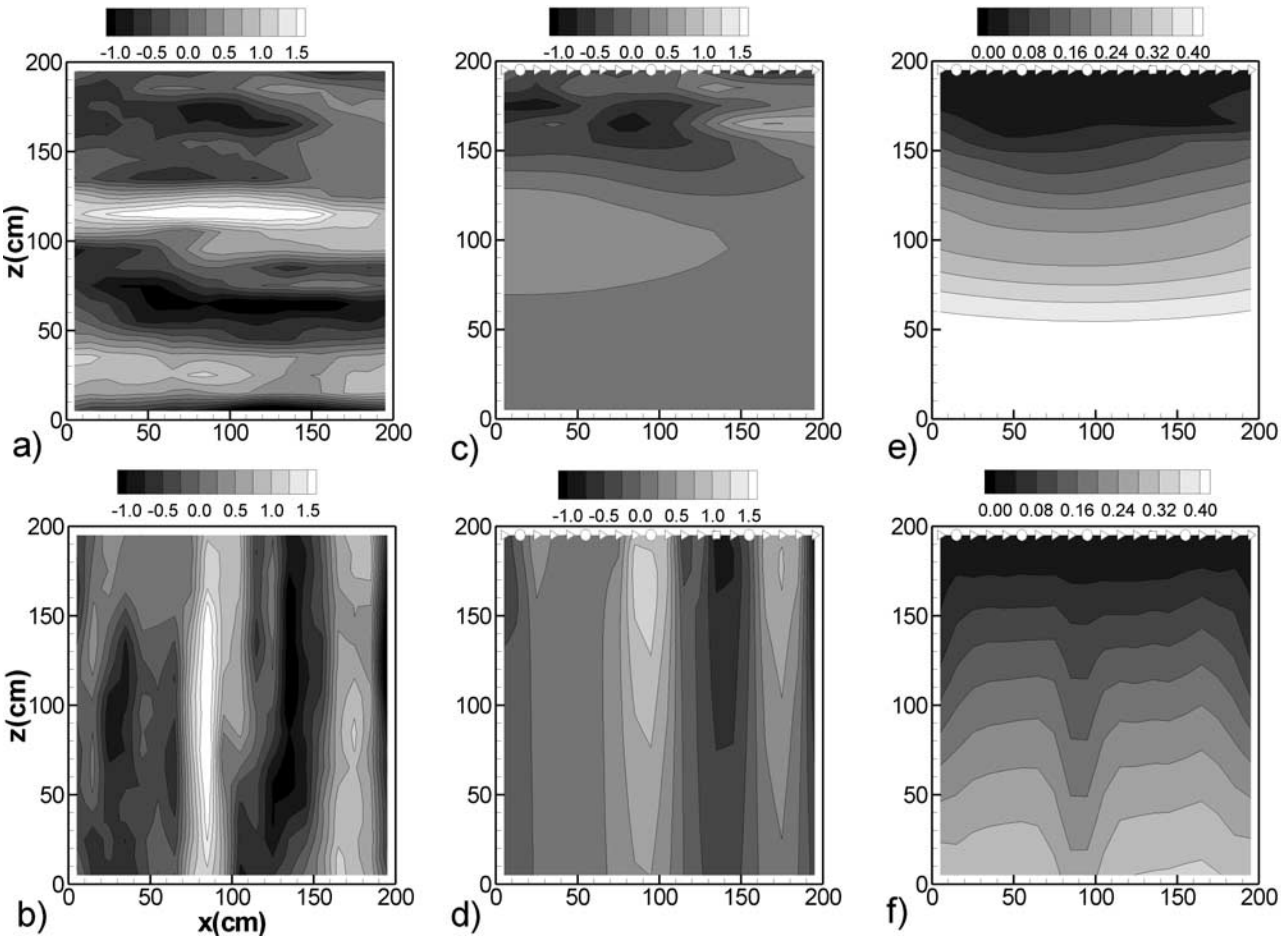

Figure 1. (a and b) True electrical conductivity perturbation fields, χ, for cases I (horizontally stratified media) and II (vertically stratified media), respectively. (c and d) Estimated conditional effective conductivity perturbation fields for cases I and II, respectively. (e and f) Conditional variances for cases I and II, respectively.

location. For example, if the conductivity at a location is known exactly, the conditional variance at that location is zero. Otherwise, the conditional variance is equal to the variance of the electrical conductivity field. Alternately, the conditional variance is smaller than the variance because of incorporation of the secondary information during the inverse modeling. Therefore the smaller the conditional variance at a given location, the better the estimate. Figure 1e shows that the surface ERT yields small conditional variances only near the land surface where electric potential measurements were taken. The variance increases rapidly with depth, indicating that the effectiveness of the survey decreases because of the stratification of the electrical conductivity field of the medium. Notice that during the generation of the electrical conductivity field, the stratification is denoted statistically by a long correlation scale in one direction and a short correlation scale in the other. Notice also that during the inversion of the ERT survey data sets for the two cases, the information about the covariance function corresponding to each case was prescribed, implying the difference in the inverse results comes solely from the nature of the inverse problem. As a consequence, Figures 1a–1f manifest the fact that orientation of stratification can affect the effectiveness of an ERT array layout. That is, when the array is perpendicular to the stratification (case II), potentials at measurement locations possess information over greater extents (depths in this study) than when the array is parallel to the stratification. Because of this fact and because most of geological formations are horizontally stratified, a down-hole ERT array is generally more effective in depicting the electrical conductivity field over a greater volume than a surface ERT array.

[20] In addition to the first two cases, case III and case IV were also investigated. In case III, two down-hole ERT arrays (19 potential electrodes and 1 current electrode) were used. For case IV, a combination of the down-hole arrays (19 potential electrodes and 1 current electrode) and one surface array (20 potential electrodes) were deployed in the hypothetical electrical conductivity field. Figure 2a illustrates the estimated conditional effective electrical conductivity field for case III. A combination of the surface and the down-hole electrode arrays (case IV) yields a higher-resolution image of the electrical conductivity field near the surface (Figure 2b). This is attributed to the additional surface-monitoring array. This conclusion is also evident in Figures 2c and 2d, where the corresponding conditional variance distribution for each case is shown.

[21] While the conditional variance provides uncertainty of the estimate, it is an ensemble statistic, which may not be appropriate for the single realization described in these

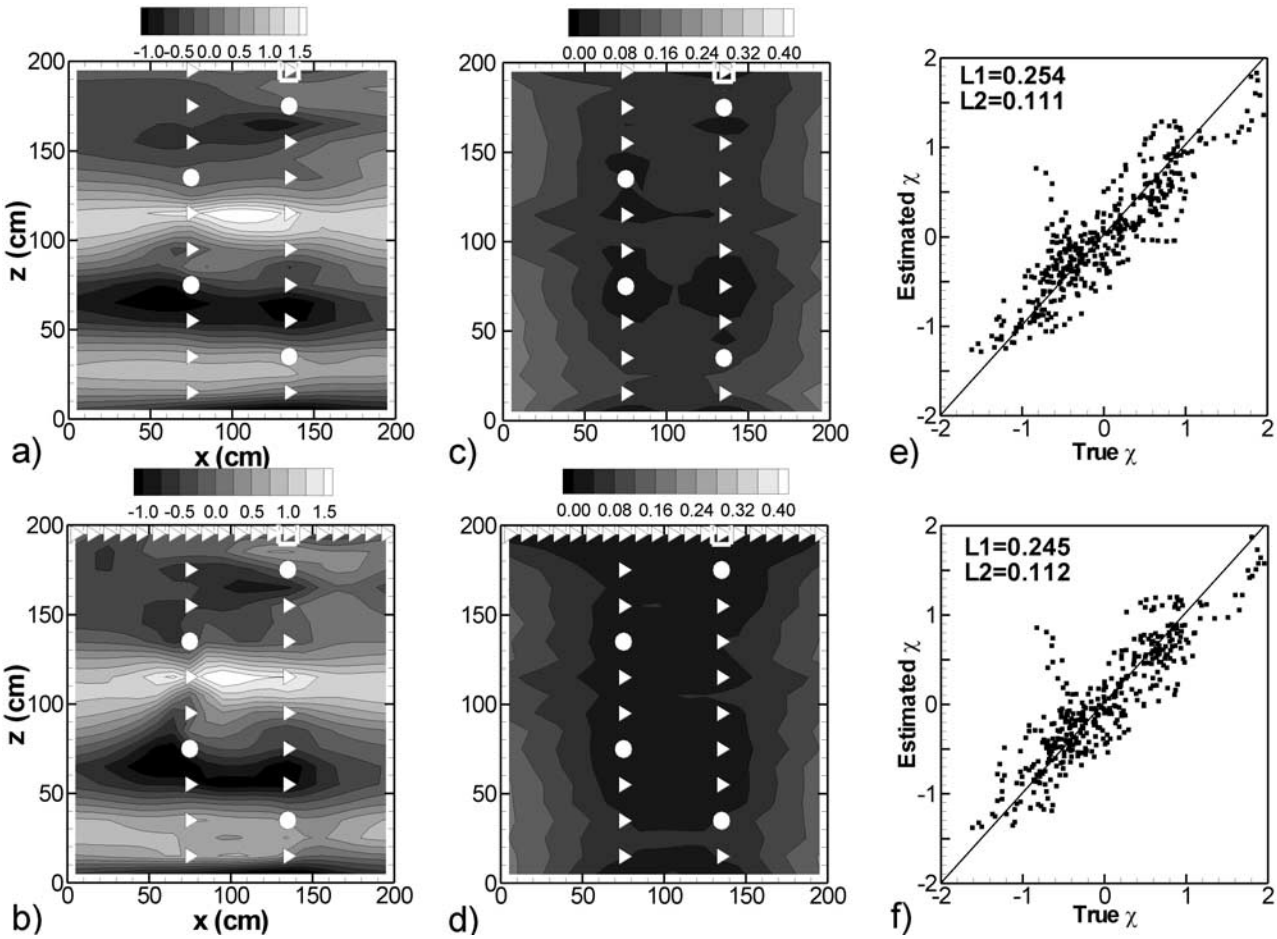

Figure 2. (a) Estimated conditional effective electrical conductivity perturbation field for case III (down-hole ERT arrays) and (b) for case IV (a combination of the surface and down-hole arrays). (c and d) Corresponding conditional variances. (e and f) Corresponding scatterplots.

examples. Better criteria to compare the estimated conductivity field with the true field are the average absolute error norm, $L1$ and the mean square error norm, $L2$, which are defined as

$$L1 = \frac{1}{N}\sum_{i=1}^{N}|\hat{\chi}_i - \chi_i| \qquad L2 = \frac{1}{N}\sum_{i=1}^{N}(\hat{\chi}_i - \chi_i)^2, \tag{10}$$

where χ_i and $\hat{\chi}_i$ represent the true and the estimated perturbation of the conditional effective electrical conductivity after a natural logarithm transformation, respectively, i indicates the element number, and N is the total number of elements in the hypothetical vadose zone. The smaller the $L1$ and the $L2$ value, the better the estimate. Figures 2e and 2f show plots of the true χ versus estimated conditional effective χ fields and the $L1$ and $L2$ values associated with the two cases. The results are consistent with those based on the conditional variance criterion. Also illustrated in Figures 2e and 2f is the discrepancy between the true and the estimate (scattering around the 45° line) caused by the limited measurements of the electric potential field.

[22] In the above inversion examples, the voltage/current measurements were assumed to be error-free and statistical parameters such as mean, variance, and correlation scales required for the inversion were assumed to be known or estimated beforehand. For hydraulic tomography, both the effects of error in measurements, and uncertainty of the statistical parameters on the estimate were investigated numerically by *Yeh and Liu* [2000] and using sandbox experiments [*Liu et al.*, 2002]. In short, they found that uncertainty of the statistical parameters does not influence the estimate significantly if sufficient and accurate secondary information is available. However, errors in point measurements of hydraulic conductivity or hydraulic head can have significant impacts on the estimate. They reported that the benefit of hydraulic tomography vanishes rapidly if the hydraulic head monitoring locations remain the same. In addition, network design issues were explored, such as the sample interval for head measurements and the location of pumping in terms of the correlation scale of the heterogeneity. We believe their results also hold for the ERT.

6. Translation of Electrical Resistivity Distribution to Water Content Distribution for Hydrological Applications

[23] Electrical resistivity tomography has been used to monitor spatial and temporal variation of soil water content

[e.g., *Daily et al.*, 1992; *Zhou et al.*, 2001; *Brainard et al.*, 2001]. During an infiltration event, the water content of geological media is generally assumed to be the only element that undergoes dramatic changes. Therefore tracking the change in the electrical resistivity has often been regarded as a useful means to delineate the change of the water content in the vadose zone. Specifically, an ERT survey is conducted on a site before an infiltration event in order to obtain the background distribution of the electrical resistivity. After the infiltration event, an ERT survey is undertaken again to acquire the electrical resistivity distribution of the wetted soils. Next, the difference between the two electrical resistivity distributions is used to interpret infiltration and the movement of the water plume, assuming a relation between the electrical resistivity and water content.

[24] In order to relate the water content to resistivity, a power law has been used:

$$\rho = \rho_o \theta^{-\mathbf{m}}. \tag{11}$$

In (11), ρ is bulk electrical resistivity, ρ_o is a fitting parameter that is related to the electrical resistivity of pore water, m is a fitting parameter, and θ denotes water content. Using (11), the difference between the natural log of the electrical resistivity before and after infiltration then becomes

$$\Delta \ln \rho = -m \Delta \ln \theta. \tag{12}$$

According to this equation, if m is constant and known precisely, then the change of $\ln\rho$ is linearly proportional to the change of $\ln\theta$. However, the change in $\ln\rho$ may not directly correspond to the change of $\ln\theta$ if m exhibits significant spatial variability. This implies that the same amount of change in moisture content may lead to different amounts of change in the electrical resistivity in different part of a medium. Notice the variability of ρ_o does not appear in equation (12). A statistical analysis based on equation (12), assuming independence between m and θ, leads to an expression for the variability in change in $\ln\rho$:

$$\mathrm{var}[\Delta \ln \rho] = M^2 \, \mathrm{var}[\Delta \ln \theta] + \Theta^2 \, \mathrm{var}[m], \tag{13}$$

where var[$\Delta\ln\theta$], var[$\Delta\ln\rho$], and var(m) are variances of $\Delta\ln\theta$, $\Delta\ln\rho$ and m, respectively. The change in mean $\ln\theta$ is denoted by Θ, and M is the mean value of m. According to equation (13), the variability of $\Delta\ln\rho$ depends on not only the variance of $\Delta\ln\theta$ but also the variance (spatial variability) of m, M, and Θ.

[25] To investigate the spatial variability of ρ_o and m in the field, the electrical resistivity as a function of the moisture content was measured for 25 samples collected from a borehole at the Sandia-Tech Vadose Zone (STVZ) infiltration field site, Socorro, New Mexico. The field site sediments are part of the Sierra Ladrones Formation, Upper Santa Fe Group. They consist of fine to coarse grained, poorly consolidated, ancestral Rio Grande axial-river deposits with intermittent layers of debris flow sediments and sedimentary layers of eolian sands (see *Brainard et al.* [2001] for a complete site description). A total of 25 samples were collected from eight 1.5-m lengths of a continuous core from a borehole at the field site.

[26] The samples were highly unconsolidated and easily disintegrated. They had to be repacked into sample rings to bulk density values determined from preliminary in situ measurements. The bulk densities were estimated to be 1.53 g cm^{-3} for fine-medium sand, 1.61 g cm^{-3} for medium-coarse sand, and 1.34 g cm^{-3} for clays. The samples were then placed in a hanging column apparatus and were allowed to reach moisture equilibrium at tensions from 100 cm down to 0 cm to obtain the main wetting curve (MWC). Also, we reversed the process by measuring the moisture retention for the main drainage curve (MDC) starting at the saturated moisture content. Pressure chambers were used to drain the samples at pressures greater than 100 cm. Moisture equilibrium was determined during imbibition by weighing the samples daily and observing changes in moisture content. Equilibrium was determined during drainage by monitoring the water level in the burette.

[27] The electrical resistivity was measured at each moisture equilibrium point for both the MWC and MDC by placing the sample in an impedance analyzer sample holder, and applying a logarithmic sweep of frequencies across the sample. A Hewlett Packard model 4129A LF [*Knight*, 1991] impedance analyzer was connected to a personal computer for automated data acquisition of impedance measurements. The impedance value corresponding to the frequency not affected by polarization at the sample/electrode interface was used to calculate the electrical resistivity. The electrical resistivity was calculated by multiplying the sample resistance by the ratio of the sample cross-sectional area to the sample length [*Knight*, 1991]. Equation (11) was then fit to the measured electrical resistivity and moisture data to determine the values for ρ_o and m. A plot of the measured electrical resistivities at each moisture content and best fit curves for the 25 cores is shown in Figure 3, where it can be seen that significant variability exists in the electrical resistivity and moisture content relation.

[28] Frequency distributions of the values for $\ln\rho_o$ and $\ln m$ are shown in Figure 4, and it appears that both $\ln\rho_o$ and $\ln m$ are approximately normally distributed. Assuming they follow lognormal distributions, the statistics for these two parameters of the core samples were determined. The geometric mean of ρ_o is 7.036 [ohm m] and the variance, standard deviation, and percent of coefficient of variation for $\ln\rho_o$ are 0.633, 0.796, and 40.8, respectively. For the parameter m, the geometric mean is 1.336, and variance, standard deviation, and percent of coefficient of variation for $\ln m$ are, 0.034, 0.185, and 63.7, respectively.

[29] A spatial statistical analysis was also conducted. Variograms for the parameters are presented in Figure 5. For $\ln\rho_o$, an exponential variogram model was selected. The sill, range, and nugget values are 0.8, 3.5 m, and 0.08, respectively. Similarly, an exponential variogram model was chosen for m. The sill, range, and nugget values for $\ln m$ are 0.043, 3.5 m, and 0.01, respectively. Statistics of the two parameters manifest their spatial variability and spatial correlation structures. Figures 6a and 6b are plots of these parameter values with depth and the lithology along the

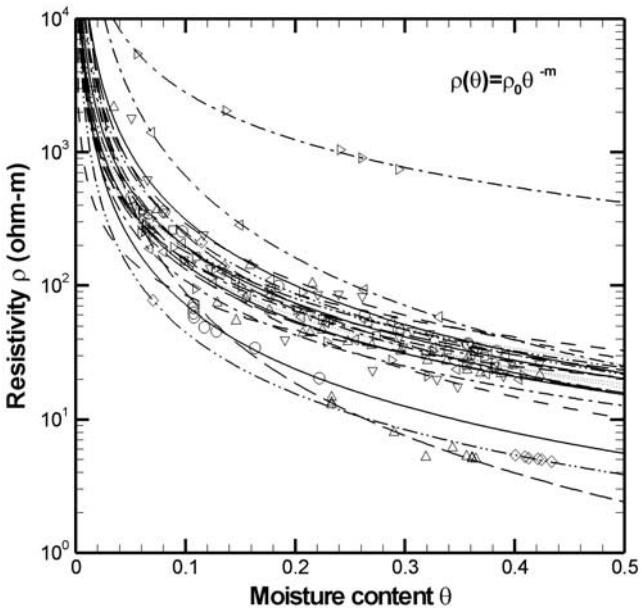

Figure 3. The electrical resistivity-moisture data and the best fit curves for samples from STVZ site at Socorro, New Mexico.

borehole. The side-by-side Figures 6a and 6b show that the spatial variation of these parameter values appears to correspond qualitatively to the lithology. Further, we found that the relation between the electrical resistivity and the moisture content did not appear to be hysteretic [*Baker*, 2001].

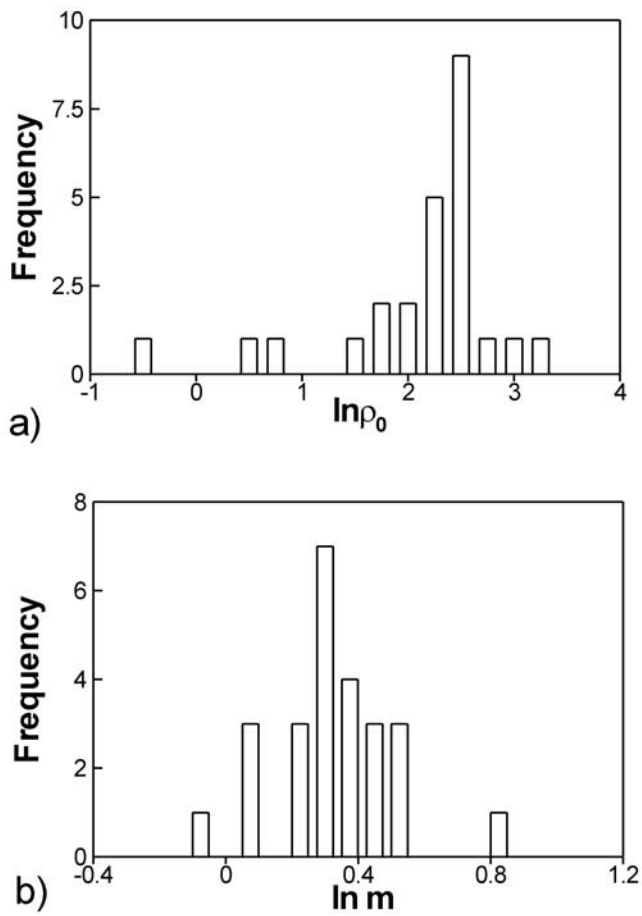

Figure 4. Frequency distributions for $\ln\rho_0$ and $\ln m$ of the STVZ data set.

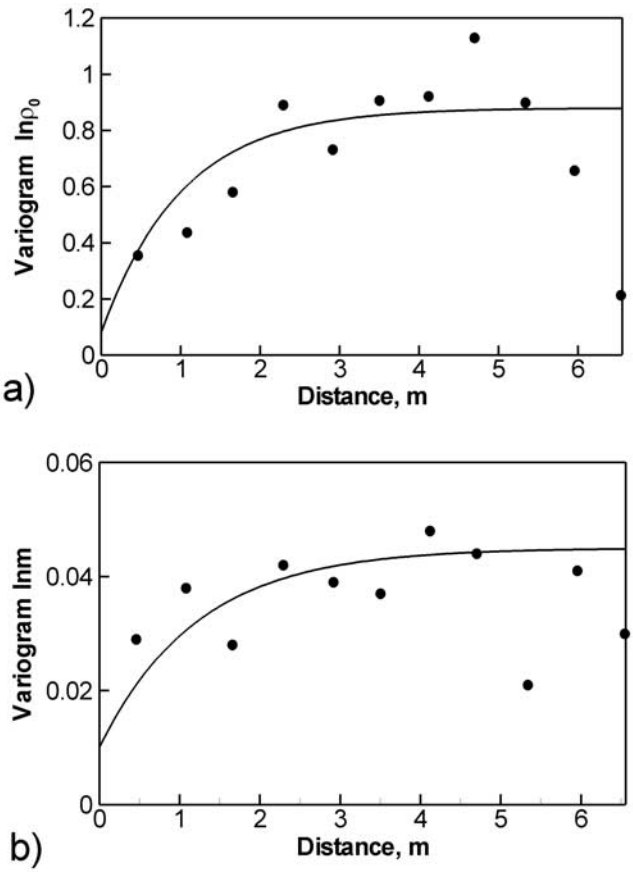

Figure 5. Variograms for (a) $\ln\rho_0$ and (b) $\ln m$ data sets at the STVZ site, showing their spatial structures.

7. Uncertainty in Hydrologic Interpretation

[30] Our field data demonstrated a significant spatial variability of the electrical resistivity and moisture content relation. In this section, the effects of this variability are investigated with regard to moisture movement, which was monitored using ERT surveys in the vadose zone.

[31] We investigated two scenarios in a hypothetical vadose zone of 200 cm × 20 cm × 200 cm. In scenario 1, the electrical resistivity field before and after infiltration was known precisely. For scenario 2, the electrical resistivity fields were estimated from a down-hole ERT survey. The hypothetical vadose zone was discretized into 200 elements, and each element had a dimension of 20 cm in both horizontal directions and 10 cm in the vertical. The unsaturated hydraulic properties of each element were assumed to be described by the Mualem-van Genuchten model [*van Genuchten*, 1980]:

$$\theta(\psi) = (\theta_s - \theta_r)[1 + (|\alpha\psi|)^a]^{(-b)} + \theta_r \tag{14a}$$

$$K(\psi) = K_s\left(1 - (|\alpha\psi|)^{(a-1)}[1 + (|\alpha\psi|)^a]^{(-b)}\right)^2 / [1 + (|\alpha\psi|)^a]^{(b/2)}, \tag{14b}$$

where ψ is the capillary pressure head, K_s is the saturated hydraulic conductivity, α and a are shape factors, and b =

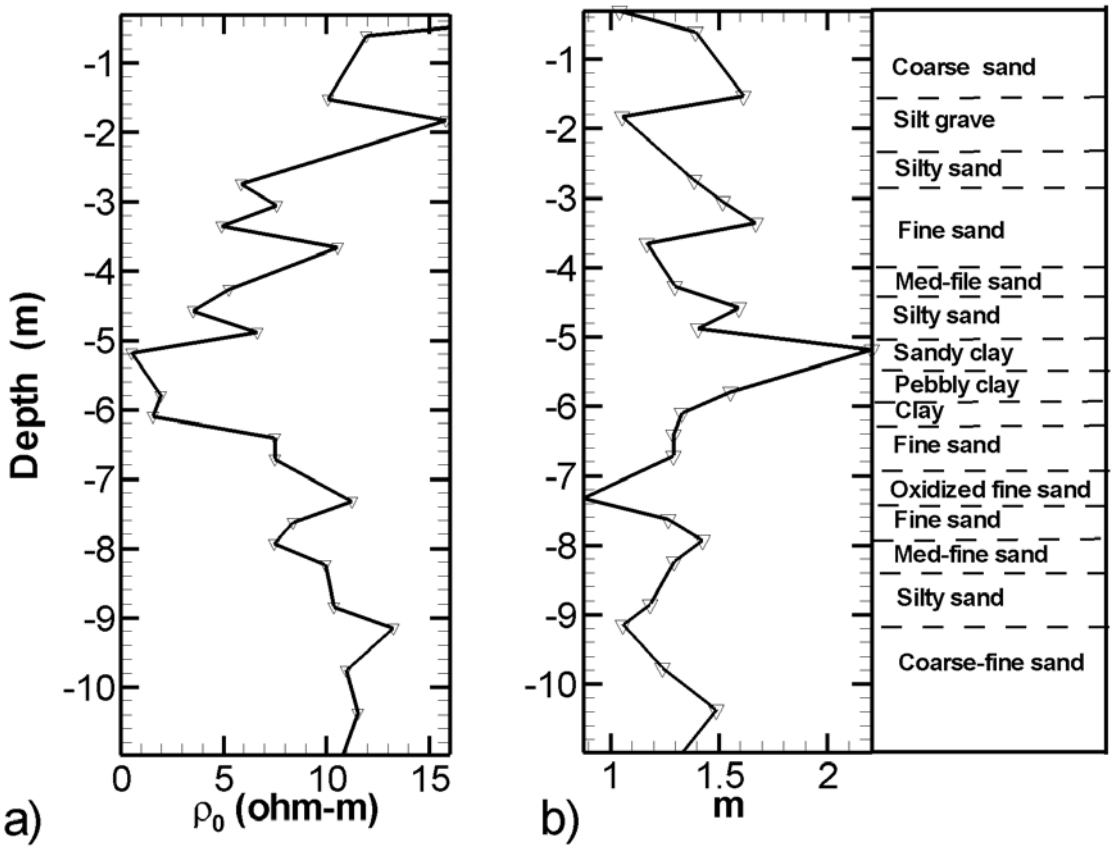

Figure 6. Spatial distributions of (a) $\rho_0 m$, and (b) lithology along a borehole at the STVZ site, Socorro, New Mexico.

$1-1/a$. The variability of saturated moisture content, θ_s, and residual moisture content, θ_r, is generally negligible; both were treated as deterministic constants with a value of 0.366 and 0.029, respectively. The parameters, K_s, α, and a, were considered as random fields with the geometric mean of 0.0063 cm s^{-1}, 0.028 cm^{-1}, and 2.0, respectively. The variances of $\ln K_s$, $\ln\alpha$, and $\ln a$ were 0.1, 0.1, and 0.01, respectively. It was also assumed that all three parameters possessed the same exponential covariance function with a horizontal correlation scale of 240 cm and a vertical correlation scale of 20 cm. Following the generation of random hydraulic parameter fields, a hydrostatic capillary pressure head distribution, with zero capillary pressure head at the bottom, was assigned to the vadose zone as the initial condition. The corresponding water content distribution was considered as the background θ distribution (Figure 7a). Next, a steady infiltration event was simulated using a finite element model for flow and solute transport in variably saturated media: Modified Method of Characteristics 3 (MMOC3) [*Srivastava and Yeh*, 1992]. The top center of the vadose zone (from $x = 80$ to 120 cm, $y = 0$ to 20 cm, and $z = 200$ cm) was treated as a constant head boundary with a capillary pressure head of -80 cm. The remainder of the surface and the two sides of the domain were considered as no-flux boundaries; the bottom was assumed to be a water table. Once the simulation of the steady flow field was completed, the resulting water content distribution was denoted as the θ distribution after infiltration (Figure 7b). The change of the $\ln\theta$ distribution before and after the infiltration was then computed and plotted in Figure 7c.

[32] In order to convert the simulated moisture content distribution to an electrical resistivity field, each element of the vadose zone was assigned a pair of ρ_o and m values using the random field generator. For the two aforementioned scenarios, three cases, A, B, and C, were considered. The m fields for the three cases were generated with a geometric mean of 1.35. The variances of $\ln m$ fields for cases A, B, and C, are 0.0, 0.033, and 0.1, respectively. While the three cases have different m fields, they have an identical ρ_o field with a geometric mean of 8.5 [ohm m] and variance of $\ln\rho_0$ equal to 0.1. Again, similar to the hydraulic parameter field, these fields have an exponential covariance structure with a horizontal correlation scale of 240 cm and the vertical correlation scale of 20 cm. Notice that although hydraulic parameter fields, ρ_o, and m fields are spatially correlated, they are mutually independent.

[33] For cases A, B, and C of scenario 1, equation (11) was used in conjunction with the generated ρ_o, and m fields, and the background θ distribution to construct the background electrical resistivity map for this hypothetical site. Similarly, the electrical resistivity distribution was also obtained after infiltration, corresponding to the θ distribution after infiltration. Then, the change in $\ln\rho$ was derived by subtracting the $\ln\rho$ after infiltration from the background $\ln\rho$. The changes in $\ln\rho$ for cases A, B, and C of scenario 1 are shown in Figures 8a, 8b, and 8c, respectively, and are plotted against $m\Delta\ln\theta$ of case A along with the values of $L1$ and $L2$ in Figures 9a, 9b, and 9c.

[34] According to Figures 7c, 8a, 8b, and 8c, the change in $\ln\rho$ reflects the change in $\ln\theta$ only if the electrical

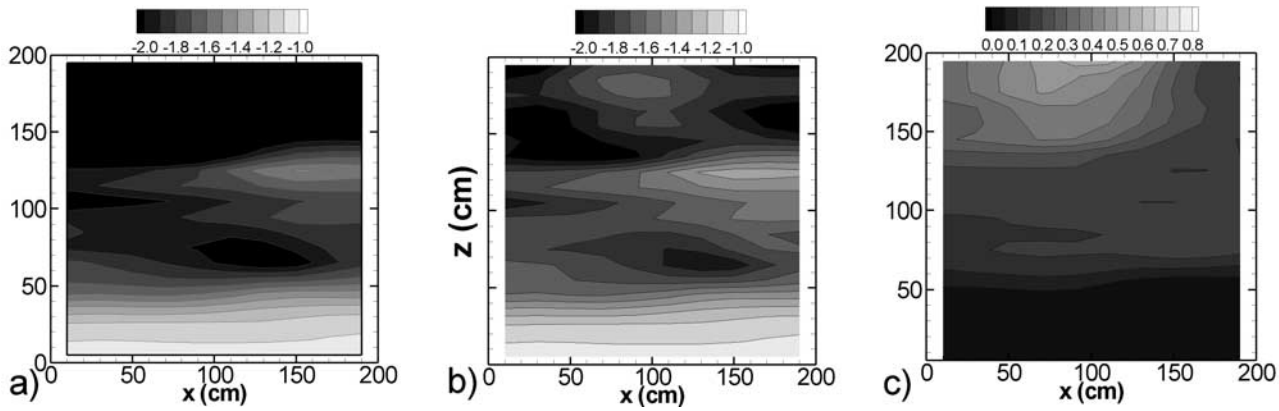

Figure 7. (a) Simulated moisture distribution (lnθ) before infiltration. (b) Simulated moisture distribution (lnθ) after infiltration. (c) Spatial distribution of change in moisture content (Δlnθ) (i.e., differences between Figures 7a and 7b).

resistivity field is known exactly at every point and m is a constant (i.e., variance of ln$m$ = 0, Figure 8a). As the variance of ln$m$ increases, the discrepancy between change in lnρ and change in lnθ increases (Figures 8b and 8c). In other words, because of the variability of the parameter m, different parts of a geological medium exhibit different amounts of change in the electrical resistivity even if they undergo the same amount of change in water content.

[35] In scenario 2, the background electrical resistivity distribution and the θ distribution after infiltration are no longer known precisely. Instead, both electrical resistivity distributions were estimated using our sequential inverse approach to interpret the simulated ERT data collected from two down-hole arrays (circles, triangles, and a square) as indicated in Figures 8d, 8e, and 8f. Specifically, in cases A, B and C of scenario 2, forward simulations of ERT surveys were conducted in the resistivity fields, created from the random ρ_0 and m fields and θ distributions before and after infiltration. The boundary conditions were set to be the same as in previous cases. These simulations yielded electrical potential measurements at specified monitoring locations of each case, which afterward were used in the inverse model to derive estimated ρ fields. The changes in lnρ for cases A, B, and C were then calculated and are

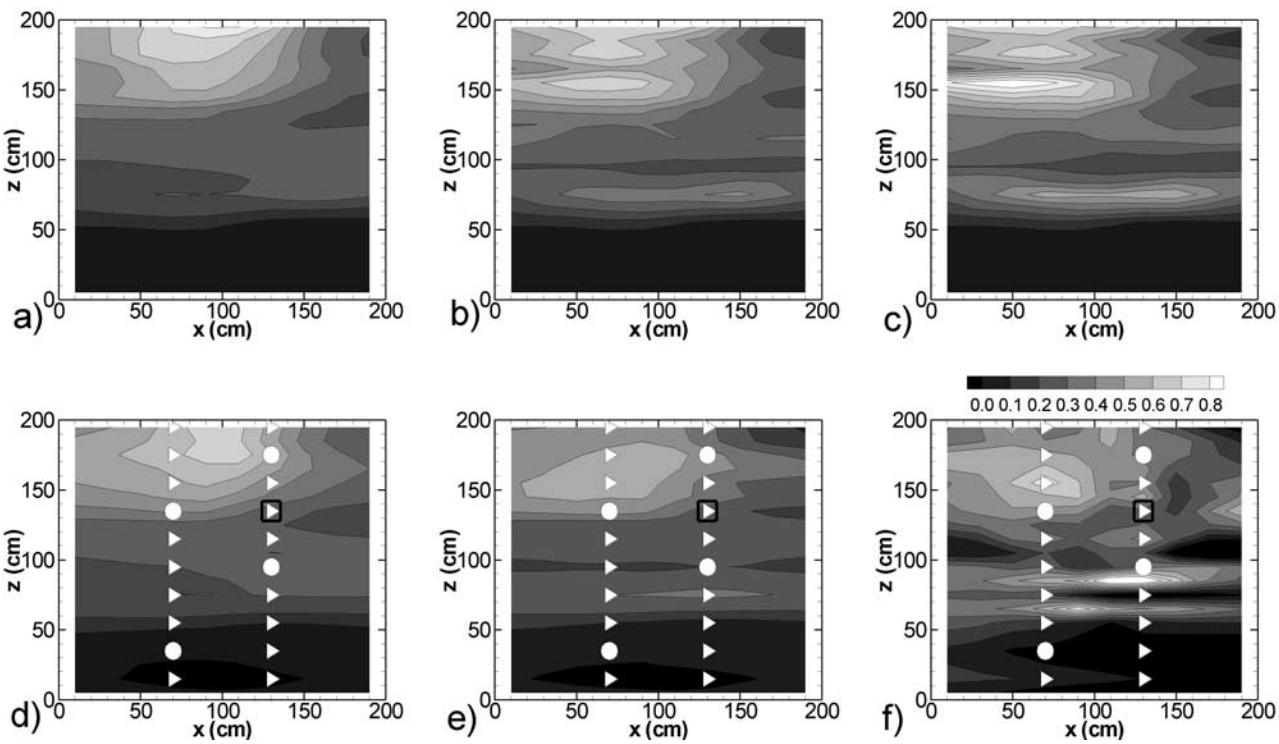

Figure 8. Distributions of changes in lnρ (a, b, and c) for cases A (the variance of m = 0.0), B (the variance of m = 0.033), and C (the variance of m = 0.1) in scenario 1(no uncertainty in lnρ), respectively. Distributions of changes in lnρ estimated from ERT surveys (d, e, and f) for cases A, B, and C of *scenario 2* (uncertainty in lnρ from ERT surveys), respectively.

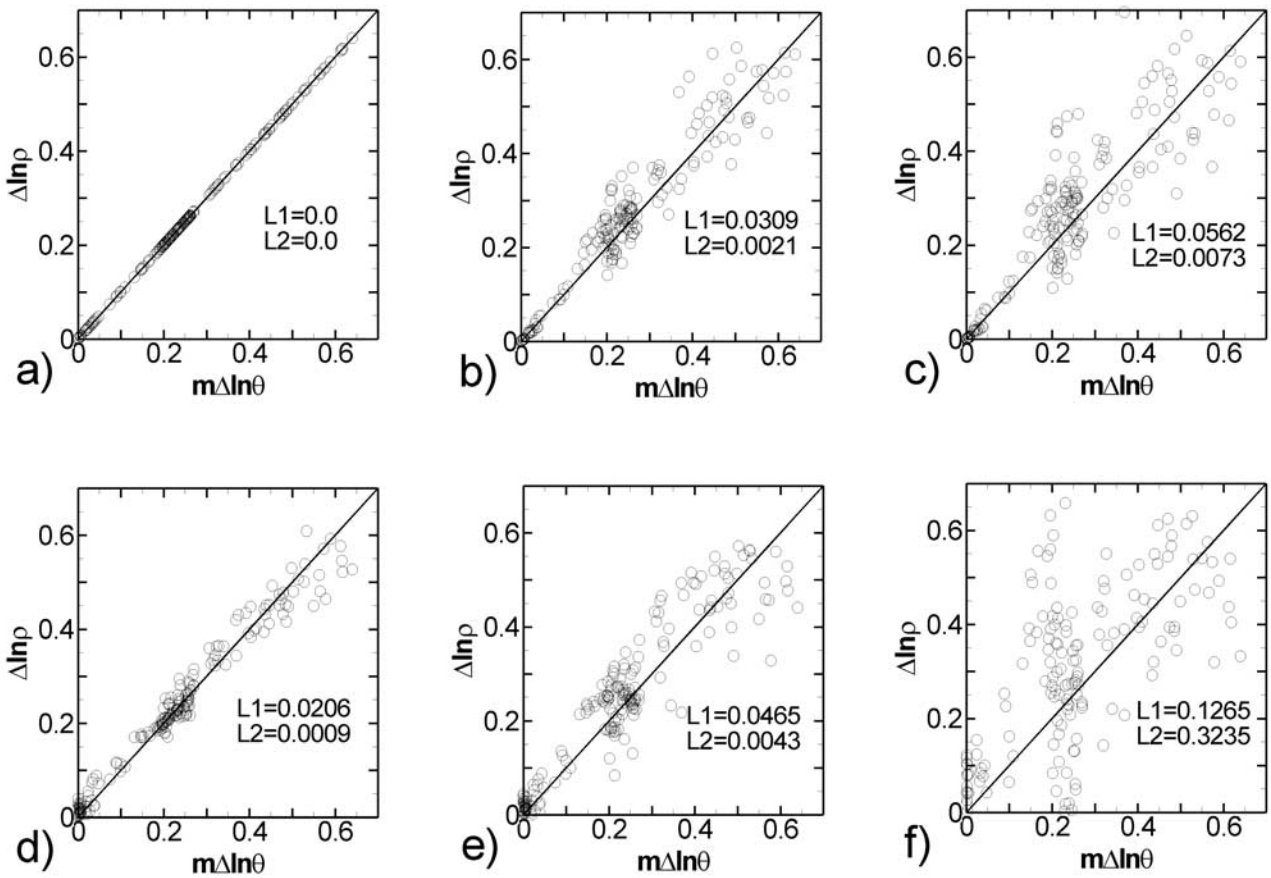

Figure 9. (a, b, and c) Scatterplots of change in lnρ versus change in lnθ corresponding to cases A, B, and C of scenario 1 (no uncertainty in lnρ) in Figures 8a, 8b, and 8c, respectively. (d, e, and f) Corresponding scatterplots for Figures 8c, 8d, and 8e, respectively, for scenario2 (with uncertainty in lnρ).

shown in Figures 8d, 8e, and 8f, respectively. They also are plotted against $m\Delta\ln\theta$ of case A of scenario 1 and are shown in Figures 9d, 9e, and 9f, along with the values of $L1$ and $L2$. Again, the measurements were considered error-free and other inputs to the model were assumed to be known exactly.

[36] In this scenario, our estimated electrical resistivity fields are uncertain because of limited information and spatial variability. A comparison between Figure 7c and Figure 8d demonstrates that even with uncertainty, the change in lnρ in case A of scenario 2 still resembles the change in lnθ when m is constant. The resemblance deteriorates as the variance of m increases, however (see Figures 8e and 8f for cases B and C of scenario 2, respectively). Notice anomalous changes in lnρ appear close to the locations (Figure 8f) where potential measurements were taken. This indicates that a great variation in m can significantly exacerbate the effect of the limited data set on the interpretation of ERT results. Consequently, caution must be taken during interpretation of the change in moisture content based on the change in the electrical resistivity alone. The accuracy of the interpretation, according to equation (13), depends on the accuracy of the ERT inversion, the mean value of m, the amount of change in mean lnθ, the variability of m, and the change in lnθ.

[37] We emphasize that our illustrations consider only the variation of parameters of the simple power law for the electrical resistivity-moisture relationship in a synthetic vadose zone. Under field conditions, many other factors can further complicate the interpretation of an ERT survey, and certainly, the validity of the power law deserves further exploration regarding the electrical resistivity-moisture relation. For instance, while the power law fits our field data quite well, it may not be suitable for other geological media. The electrical resistivity is also well known to be sensitive to salt concentration, clay content, ion exchange, temperature [*Keller*, 1987] and other site-specific attributes.

[38] While the electrical resistivity was assumed to be locally isotropic in this study, in the field it can be anisotropic and measurement-scale dependent. The electrical resistivity anisotropy of a medium at a given measurement scale, similar to the hydraulic conductivity anisotropy, is an artifact caused by averaging distinct electrical resistivity values of layers of material at scales smaller than the measurement scale. The anisotropy therefore depends on the average length and thickness of the layers, and the variance of each layer's electrical resistivity, which may vary with the scale of measurement (or the size of discretization of the domain used in ERT inversion). In general, the electrical

resistivity is greatest in the direction perpendicular to layering and least in the direction parallel to layering. Moreover, because the electrical resistivity of each layer can vary with moisture content and therefore among the layers, the anisotropy of the averaged bulk electrical resistivity is expected to vary with the moisture content. Specifically, the electrical resisitivity anisotropy ratio is defined as the ratio of the bulk electrical resistivity of electric current flow perpendicular to bedding to the resistivity of electrical current flow parallel to bedding. The anisotropy ratio will increase as the medium becomes less saturated in a manner similar to the moisture-dependent anisotropy in unsaturated hydraulic conductivity described by *Yeh et al.* [1985a, 1985b, 1985c].

[39] These possible complications necessitate further theoretical and experimental investigations of the fundamental electrical resistivity-moisture relation. Their effects on the inversion of ERT and its hydrological interpretation deserve further exploration. Finally, while the ability of ERT surveys for detecting changes in moisture content is attractive, we must point out that many hydrological analyses demand accurate measurements of moisture content distributions, not just the monitoring of soil moisture changes.

8. Conclusion

[40] A sequential, geostatistical inverse approach for hydraulic tomography was adapted for electrical resistivity tomography. The sequential inverse approach mimics the sequential ERT data collection scheme commonly employed in a traditional field survey. The inverse method constrains the estimate of the electrical resistivity field by including borehole measurements of the electrical resistivity, in addition to potential measurements from the ERT survey, and information of geological structures through the statistic spatial covariance. The sequential approach is computationally efficient, allows fine-grid discretization of the solution domain, and permits sequential inclusion of different data sets. Furthermore, the conditional variance in the inverse model quantifies uncertainty in the estimate caused by the spatial variability of the electrical resistivity, uncertainty in measurement errors, and a limited number of data sets.

[41] Through numerical experiments based on our inverse approach, we showed that geological bedding affects effectiveness of the sampling array of ERT. Sampling perpendicular to bedding (down-hole array) increases the resolution of the electrical resistivity estimate because of the long correlation in the direction parallel to bedding. Conversely, the effectiveness of the surface array (sampling parallel to bedding) is restricted to a shallow depth because of the long correlation scale along bedding and the short correlation scale in the direction perpendicular to bedding. Significant variability of the electrical resistivity-moisture relation was observed in our field samples. Both the theoretical analyses and numerical experiments suggest that such a spatially varying relation can exacerbate the level of uncertainty in the interpretation of change of moisture content based on the estimated change in the electrical resistivity. These results call for additional studies of the underlying physics of the electrical resistivity-moisture relation and its spatial variation. Last, development of better methodologies is needed for incorporating this variability in the interpretation of the ERT survey, such that ERT can be an effective monitoring tool for vadose zone processes.

[42] **Acknowledgments.** This research is funded in part by a DOE EMSP96 grant through Sandia National Laboratories (contract AV-0655#1) and a DOE EMSP99 grant through University of Wisconsin, A019493. At Sandia National Laboratories, work was supported by DOE EMSP under contact DE-AC04-94 AL85000. We also gratefully acknowledge our colleague, Martha P.L. Whitaker, for proofreading this document in its various states of completion. Many thanks are extended to two reviewers for providing critical comments to improve the paper. In particular, we are greatly indebted to Andreas Kemna, who provided a meticulous, insightful, constructive, and open-minded review of our manuscript.

References

Baker, K., Investigation of direct and indirect hydraulic property laboratory characterization methods for heterogeneous alluvial deposits: Application to the Sandia-Tech vadose zone infiltration test site, Masters thesis, New Mexico Inst. of Mining and Tech., Socorro, N. M., 2001.

Brainard, J. R., R. J. Glass, D. L. Alumbaugh, L. Paprocki, D. LaBrecque, X. Yang, T.-C. J. Yeh, K. E. Baker, and C. A. Rautman, The Sandia-Tech vadose zone facility: Experimental design and data report of a constant flux infiltration experiment, internal report, Sandia Natl. Lab., Albuquerque, N. M., 2001.

Carle, S., A. Ramirez, W. Daily, R. Newmark, and A. Tompson, High-performance computation and geostatistical experiments for testing the capabilities of 3D electrical resistance tomography, paper presented at SAGEEP 1999 Conference, Environ. And Eng. Geophys. Soc., Oakland, Calif., 14–18 March 1999.

Daily, W., A. Ramirez, D. LaBrecque, and J. Nitao, Electrical resistivity tomography of vadose water movement, *Water Resour. Res.*, *28*(5), 1429–1442, 1992.

Ellis, R. G., and S. W. Oldenburg, The pole-pole 3-D dc resistivity inverse problem: A conjugate gradient approach, *Geophys. J. Int.*, *119*, 187–194, 1994.

Gavalas, G. R., P. C. Shan, and J. H. Seinfeld, Reservoir history matching by Bayesian estimation, *Soc. Pet. Eng. J.*, *261*, 337–350, 1976.

Gelhar, L. W., *Stochastic Subsurface Hydrology*, Prentice-Hall, Englewood Cliffs, N. J., 1993.

Gutjahr, A., Fast Fourier transforms for random field generation, project report for Los Alamos grant, contract 4-R58-2690R, 106 pp., N. M. Inst. of Min. and Technol., Socorro, 1989.

Gutjahr, A., B. Bullard, S. Hatch, and D. L. Hughson, Joint conditional simulations and the spectral approach to flow modeling, *Stochastic Hydrol. Hydraul.*, *8*(1), 79–108, 1994.

Hanna, S., and T.-C. J. Yeh, Estimation of co-conditional moments of transmissivity, hydraulic head, and velocity fields, *Adv. Water Resour.*, *22*, 87–93, 1998.

Hoeksema, R. J., and P. K. Kitanidis, An application of the geostatistical approach to the inverse problem in two-dimensional groundwater modeling, *Water Resour. Res.*, *20*(7), 1003–1020, 1984.

Hughson, D. L., and T.-C. J. Yeh, A geostatistically based inverse model for three-dimensional variably saturated flow, *Stochastic Hydrol. Hydraul.*, *12*(5), 285–298, 1998.

Hughson, D. L., and T.-C. J. Yeh, An inverse model for three-dimensional flow in variably saturated porous media, *Water Resour. Res.*, *36*(4), 829–839, 2000.

Keller, G. V., Rock and mineral properties, in *Electromagnetic Methods in Applied Geophysics*, *Invest. Geophys.*, vol. 3, *Theory*, edited by M. N. Nabighian, pp. 13–51, Soc. of Explor. Geophys., Tulsa, Okla., 1987.

Kitanidis, P. K., Comment on "A reassessment of the groundwater inverse problem" by D. McLaughlin and L. R. Townley, *Water Resour. Res.*, *33*(9), 2199–2202, 1997.

Kitanidis, P. K., and E. G. Vomvoris, A geostatistical approach to the inverse problem in groundwater modeling and one-dimensional simulations, *Water Resour. Res.*, *19*(3), 677–690, 1983.

Knight, R., Hysteresis in the electrical resistivity of partially saturated sandstones, *Geophysics*, *56*, 2139–2147, 1991.

Li, Y., and D. W. Oldenburg, Inversion of 3D dc-resistivity data using an approximate inverse mapping, *Geophys. J. Int.*, *116*, 527–537, 1994.

Li, Y., and D. W. Oldenburg, Incorporating geological dip information into geophysical inversions, *Geophysics*, *65*, 148–157, 2000.

Liu, S., T.-C. J. Yeh, and R. Gardiner, Effectiveness of hydraulic tomography: Sandbox experiments, *Water Resour. Res.*, *38*(4), 1034, doi:10.1029/2001WR000338, 2002.

McLaughlin, D., and L. R. Townley, A reassessment of the groundwater inverse problem, *Water Resour. Res.*, *32*(5), 1131–1161, 1996.

National Research Council, *Seeing Into the Earth: Noninvasive Characterization of the Shallow Subsurface for Environmental and Engineering Application*, Natl. Acad. Press, Washington D. C., 2000.

Oldenburg, D. W., and Y. Li, Estimating depth of investigation in dc resistivity and Ip surveys, *Geophysics*, *64*, 403–416, 1999.

Sharma, P. V., *Environmental and Engineering Geophysics*, Cambridge Univ. Press, New York, 1997.

Srivastava, R., and T.-C. J. Yeh, A three-dimensional numerical model for water flow and transport of chemically reactive solute through porous media under variably saturated conditions, *Adv. Water Resour.*, *15*, 275–287, 1992.

Sun, N. Z., *Inverse Problems in Groundwater Modeling*, Kluwer Acad., Norwell, Mass., 1994.

van Genuchten, M. T., A closed-form equation for predicting the hydraulic conductivity of unsaturated soils, *Soil Sci. Soc. Am. J.*, *44*, 892–898, 1980.

Vargas-Guzman, A. J., and T.-C. J. Yeh, Sequential kriging and cokrging: Two powerful geostatistical approaches, *Stochastic Environ. Res. Risk Assess.*, *13*, 416–435, 1999.

Yeh, T.-C. J., Scale issues of heterogeneity in vadose-zone hydrology, in *Scale Dependence and Scale Invariance in Hydrology*, edited by G. Sposito, Cambridge Univ. Press, New York, 1998.

Yeh, T.-C. J., and S. Y. Liu, Hydraulic tomography: Development of a new aquifer test method, *Water Resour. Res.*, *36*(8), 2095–2105, 2000.

Yeh, T.-C. J., L. W. Gelhar, and A. L. Gutjahr, Stochastic analysis of unsaturated flow in heterogeneous soils, 1, Statistically isotropic media, *Water Resour. Res.*, *21*(4), 447–456, 1985a.

Yeh, T.-C. J., L. W. Gelhar, and A. L. Gutjahr, Stochastic analysis of unsaturated flow in heterogeneous soils, 2, Statistically anisotropic media, *Water Resour. Res.*, *21*(4), 457–464, 1985b.

Yeh, T.-C. J., L. W. Gelhar, and A. L. Gutjahr, Stochastic analysis of unsaturated flow in heterogeneous soils, 3, Observations and applications, *Water Resour. Res.*, *21*(4), 465–471, 1985c.

Yeh, T.-C. J., A. L. Gutjahr, and M. Jin, An iterative cokriging-like technique for groundwater flow modeling, *Groundwater*, *33*(1), 33–41, 1995.

Yeh, T.-C. J., M. Jin, and S. Hanna, An iterative stochastic inverse method: Conditional effective transmissivity and hydraulic head fields, *Water Resour. Res.*, *32*(1), 85–92, 1996.

Yeh, W. W.-G., Review of parameter identification procedures in groundwater hydrology: The inverse problem, *Water Resour. Res.*, *22*(1), 95–108, 1986.

Zhang, J., and T.-C. J. Yeh, An iterative geostatistical inverse method for steady flow in the vadose zone, *Water Resour. Res.*, *33*(1), 63–71, 1997.

Zhang, J., R. L. Mackie, and T. Madden, 3-D resistivity forward modeling and inversion using conjugate gradients, *Geophysics*, *60*, 1313–1325, 1995.

Zhou, Q. Y., J. Shimada, and A. Sato, Three-dimensional spatial and temporal monitoring of soil water content using electrical resistivity tomography, *Water Resour. Res.*, *37*(2), 273–285, 2001.

D. Alumbaugh, Department of Civil and Environmental Engineering, University of Wisconsin-Madison, 1415 Engineering Drive, Madison, WI 53706, USA. (alumbaugh@engr.wisc.edu)

K. Baker, Idaho National Engineering and Environmental Laboratory, P.O. Box 1625, MS 2107, Idaho Falls, ID 83415-2107, USA. (bakeke@inel.gov)

J. R. Brainard and R. J. Glass, Sandia National Laboratories, P.O. Box 5800, MS 0735, Albuquerque, NM 87185-0735, USA. (jrbrain@sandia.gov; rjglass@sandia.gov)

D. LaBrecque, MultiPhase Technologies, 310 Rebecca Drive, Sparks, NV 89436, USA. (dlabrec887@yahoo.com)

S. Liu, Allen, Stephenson and Associates, 1130 E. Missouri Avenue, Phoenix, AZ 85014, USA. (shuyun_liu@yahoo.com)

T.-C. J. Yeh, Department of Hydrology and Water Resources, University of Arizona, P.O. Box 210011, Tucson, AZ 85721-0011, USA. (yeh@hwr.arizona.edu)